Title
A REVIEW OP THE PHYSICAL CHARACTERISTICS OF PION BEAMS

Authors
Raju, Mudundi R.
Richman, Chaim
Curtis, Stanley B.

Publication Date
1967-03-17

UCRL-17441

University of California

Ernest O. Lawrence Radiation Laboratory

A REVIEW OF THE PHYSICAL CHARACTERISTICS OF PION BEAMS

Berkeley, California

DISCLAIMER

Proceedings of the
First International Symposium on the
Biological Interpretation of Dose from
Accelerator-Produced Radiation,
Berkeley, March 13-16, 1967

UCRL-17441
Preprint

UNIVERSITY OF CALIFORNIA

Lawrence Radiation Laboratory
Berkeley, California

AEC Contract No. W-7405-eng-48

A REVIEW OF THE PHYSICAL CHARACTERISTICS OF PION BEAMS

Mudundi R. Raju, Chaim Richman, and Stanley B. Curtis

March 17, 1967

A REVIEW OF THE PHYSICAL CHARACTERISTICS OF PION BEAMS*

Mudundi R. Raju, Chaim Richman, and Stanley B. Curtis

Donner Laboratory and Lawrence Radiation Laboratory
University of California, Berkeley, California

and

Graduate Research Center of the Southwest
Dallas, Texas

March 17, 1967

INTRODUCTION

Localization of radiation dose in a region of interest, for example, in tumor tissue, while sparing the normal tissue is one of the essential requirements for radiotherapy. It has been known for a long time that the blood supply has a great effect on the sensitivity of tissue to radiation, and clinical studies have shown that tumors with good blood supply are more sensitive to radiation. In most types of neoplasma there are likely to be cells deficient in oxygen. As such cells are relatively insensitive to radiation, they survive the usual forms of radiotherapy and cause recurrence of the tumor growth. However, this oxygen effect diminishes considerably for high-LET radiations. Hence the radiation to be used for cancer therapy preferably should have the properties of delivering a highly localized radiation dose of high LET. Conventional x rays have limited penetrating qualities and are of low LET; hence they cause damage preferentially to the oxygenated tissue. High-energy radiation such as ^{137}Cs, ^{60}Co, and high-energy x rays and electrons have better penetrating qualities, but again the LET is low.

The fast neutrons of modal energy 6 MeV have penetration similar to that of 250 kVP x rays, but in interacting with tissue produce recoil protons with LET high enough to overcome the oxygen effect considerably.

A few years after the discovery of the neutron, fast neutrons obtained from small cyclotrons then developed at Berkeley were tried[1] for tumor therapy but without success because of the lack of knowledge in radiobiology and the then erratic operation of the cyclotrons.[2] More work with fast neutrons is now being done at Hammersmith Hospital, London, and this technique may prove to be beneficial for tumor therapy. Unfortunately, there is always a necessary compromise between getting a higher LET by using low-energy neutrons and getting better depth dose by using high-energy neutrons.

---

*Work done under the auspices of the U. S. Atomic Energy Commission, the American Cancer Society, and the Office of Naval Research.

The highly accelerated heavy charged particles such as protons, deuterons, and α particles are of special interest because of their physical properties. Since the mass of singly charged heavy particles is many times that of the electron, the angle of Coulomb scattering for a given velocity is reduced approximately by the ratio of the masses of the incident particle and the electron; thus undesirable side scattering can be reduced to a minimum. The radiation fields of heavy charged particles can also be shaped with greater precision than those of x rays and gamma rays. The heavy-charged-particle beam has a definite range of penetration that depends on its energy. It proceeds through a medium in very nearly a straight line; the increase in dose delivered by it as the particles slow down gives rise to a sharp maximum known as the Bragg peak near the end of the range. Hence intense irradiation of a strictly localized region within the body is possible with relatively small dose at the skin.

However, the Bragg peak is too narrow to permit uniform irradiation of most tumors, and the LET at the Bragg peak position is also much lower than one would normally[3] expect (for example at the Bragg peak of 910 MeV α beam the LET corresponding to the modal energy is ~ 10 keV/μ). It is possible to irradiate the entire tumor region by transforming the Bragg peak into flat maxima using variable absorbers, but when this is done the LET will be lowered further. Hence heavy charged particles such as protons, deuterons, and α particles may not provide much oxygen advantage for cancer therapy; however, they are very useful for hypophysectomy in which anoxic cells are not involved. Heavier ions such as neon may prove to be useful for tumor therapy.[4]

The negative pi mesons (pions) are also heavy particles, and have a mass 276 times the electron mass. When a negative pion is brought to rest in a medium, say tissue, it is captured by a constituent nucleus, which explodes into a "star" consisting of short-range and heavily ionizing fragments capable of delivering a large localized radiation dose resulting in an augmented Bragg peak. The heavily ionizing fragments should be capable of overcoming the oxygen effect considerably. The pion capture can be made to take place in the tumor by proper selection of the pion energy. Negative pions pass through healthy tissue as minimum ionizing particles of very low LET (< 1 keV/μ) and stop in the tumor region, delivering a large localized dose at much higher LET. Hence the use of negative pions in principle should be very promising for therapeutic applications. A few people, including Richman appreciated this possibility as early as 1952. Fowler and Perkins calculated the dosage to be expected from negative pions in tumors and in the surrounding tissue.[5] Their results clearly demonstrate that for negative-pion beams, the dose delivered in the tumor should be many times that in adjoining regions. The presently available negative-pion beams are low in intensity compared with that required for therapeutic applications. At present there are four groups in the world working on this problem: Lawrence Radiation Laboratory, Berkeley; Brookhaven National Laboratory; Wills Physics Laboratory, England; and CERN, Switzerland. The pion beam at LRL at present is the most intense ($\approx 10^6$/sec) with reasonably low background. The work at the above-mentioned places will be reviewed briefly and a detailed up-to-date account of the work that has been done at this Laboratory is presented here. Some of our results have already been published,[6-9] and a short account of these published results is also included here.

INTERACTION OF CHARGED PIONS WITH TISSUE

Charged pions travel through tissue similarly to any heavy charge particle, and stop after traveling a given range that depends on energy; e.g., a 50-MeV pion travels through about 10 cm of tissue. Unlike other charged particles like electrons or protons, the charged pion is unstable; it decays in free space into a muon and a neutrino with a lifetime of $\approx 2\times10^{-8}$ sec. Hence there will always be a contamination of muons in a pion beam. The characteristic

difference in behavior between a positive and a negative pion occurs at the end of the range. When the positive pion comes to rest, the coulomb repulsion between its positive charge and that of the nucleus keeps it from interacting with the nucleus. It goes through two decay processes:

$$\pi^+ \rightarrow \mu^+ + \nu$$

$$\mu^+ \rightarrow e^+ + \nu + \bar{\nu}.$$

The ν and $\bar{\nu}$ are neutrinos and do not contribute to the dosage. The μ^+ is a short-range 4.12-MeV muon which contributes a small dose. The positron has a distribution in energy with a peak around 30 MeV. Examples of this type of decay are shown in Fig. 1.

Tissue is composed mainly of hydrogen, carbon, nitrogen, and oxygen; when a negative pion is brought to rest in such a medium, it may be captured by any one of these atoms. When captured by hydrogen, however, the resulting neutral mesic atom diffuses through the medium and when it gets close to a heavier nucleus, the pion is transferred to it because the resulting energy is lower. As a result, the pion is captured by the main tissue elements and cascades down the atomic levels to the ground state of the atom in a time that is short compared with its lifetime. From the ground state it is captured by the constituent nucleus, which explodes into a star consisting of short-range heavily ionizing fragments. In such interactions, about 20% of the total rest-mass energy (140 MeV) appears in the form of α particles, protons, and heavier fragments with ranges less than 1 mm in tissue. A further 40 MeV is expended in breaking up the nucleus, and the remaining 70 MeV is carried off by neutrons.[10] A few examples of negative-pion capture in carbon, nitrogen, or oxygen as observed in photographic emulsions are shown in Fig. 2.

The type of disintegration of a nucleus such as that of carbon and nitrogen has been studied with a diffusion cloud chamber,[11] and considerable energy was found to be in the ionizing fragments of the light elements.

The dominant reaction for carbon (accounting for $\approx 25\%$ of the captures) is

$$\pi^- + {}^{12}C \rightarrow 2\alpha + 1p + 3n.$$

The dominant reaction in nitrogen (19% of the captures) is

$$\pi^- + {}^{14}N \rightarrow 3\alpha + 2n.$$

The other reactions yield from zero to five charged particles, which at times include a heavy ion.

The relative frequency with which different elements capture pions is closely proportional to their relative abundance by mass. In bone-free parts of the body we expect 73% of the captures to be in O, 20% in C, and 3% in N, which leaves only 4% in heavier atoms. It is important, therefore, to know the characteristics of capture in oxygen nuclei. Mayes and Fowler made measurements on tracks of particles stopping in wet and dry emulsions in order to get the data on pions captured in oxygen alone.[10] They found that interactions with oxygen produce tracks of multiply-charged particles. The common form of disintegration of oxygen is into three α particles and a proton. The energy partition for π^- capture in water as given by Fowler[10] is shown in Table 1.

Table 1. Energy partition for π^- capture in water.

	MeV
Rest mass of π^-	139.6
Average binding energy	40.0
Kinetic energy	
$Z > 2$	4.5 ± 0.5
$Z = 2$	8.0 ± 0.4
$Z = 1$	16.5 ± 0.6
Neutrons	70.0
	139.0

CALCULATED ENERGY-LOSS DISTRIBUTIONS AND BRAGG CURVES

Mayes and Fowler also measured the differential energy spectra of the various particles emitted in the nuclear interaction of the negative pion with the oxygen nucleus. From these data it is possible to calculate the energy-loss distribution for a point in the stopping-pion region.[12] If some reasonable assumptions are made about the momentum spread of the incident beam and the amount of contamination by muons and electrons, the contribution from these sources can be included. The results of such a calculation are shown in Fig. 3. Conditions here were chosen to parallel those existing in the meson cave of the Berkeley cyclotron. The incident particle beam momentum was chosen as 190 MeV/c with a Gaussianly distributed momentum spread of standard deviation 5 MeV/c. The incident beam was chosen to have a 25% electron and a 10% muon contamination. The point of computation was the center of the star region at 25.5 cm of water. The contributions from the various components in the beam are shown in the figure.

The integral under the curve is proportional to the dose deposited at the computation point. If these integrals are computed for various depths and normalized to the entrance dose, a central-axis depth-dose curve (Bragg curve) can be constructed. The result of such integrations is shown for the contaminated beam in Fig. 4. The contributions of the various components are indicated. Our beam has such a large cross section (50 cm^2) that multiple-scattering corrections are negligible on the central axis. Because of the broad distribution in incident momenta, straggling corrections are negligible compared with the range spread due to the momentum distribution. It is seen from the figure that the peak-to-plateau dose ratio rises to almost 3:1 and that the width of the peak is about 4 cm.

For comparison, the depth-dose distribution for pure pions is shown in Fig. 5. Here the width of the peak is about the same as for the contaminated beam, but the peak-to-plateau dose ratio has risen to almost 3.5:1.

PRODUCTION OF PION BEAMS

Pions can be produced in a nuclear interaction by any strongly interacting particle if its energy is great enough. They are generally produced by a primary beam of protons. Our experiments at Berkeley are carried out at the 184-inch synchrocyclotron. This machine provides an accelerated beam of 732-MeV protons that in their outer orbit strike a 5-cm thick beryllium target and produce neutral, positive, and negative pions. The experimental arrangement is shown in Fig. 6. The negative pions are deflected out of the cyclotron by the cyclotron fringe field, and after leaving the cyclotron tank through a window, enter a small quadrupole focusing magnet (meson quad), then along a channel (dashed line in Fig. 6) through the main cyclotron shielding (hatched area). The pions then enter the meson cave, where various arrangements of magnets are used for energy selection and focusing of the pion beam. A bending magnet is used for momentum selection. The cyclotron produces pions in a range of energies from 0 to about 450 MeV (the upper limit being determined by the energy of the primary proton beam). In all our experiments, we used pions of energy around 90 MeV, because at this energy the yield of pions is good with reasonably low background. In the change from a negative to a positive pion beam, all the magnetic fields, including that of the cyclotron, are reversed. The magnetic-lens system remains unchanged for pions of the same energy, regardless of charge.

The negative pions are produced in the reaction of the proton beam with the neutrons in the beryllium nucleus:

$$p + n \rightarrow p + p + \pi^-.$$

The positive pions are produced in two ways:

$$p + n \rightarrow n + n + \pi^+$$

$$p + p \rightarrow p + n + \pi^+ .$$

Neutral pions are also produced. They have a very short lifetime, $\approx 10^{-16}$ sec, and decay into two γ rays in the target. The gamma rays get converted into electron-positron pairs that go mainly in the forward direction. The electrons from this conversion constitute the electron background in the negative-pion beam.

PHYSICAL MEASUREMENTS

Some of the early measurements of isodose curves of a 70-MeV pion beam obtained from the 600-MeV proton beam at the CERN cyclotron have been reported by Baarli.[13] The beam had a 30% contamination of muons and electrons. The dose at the Bragg peak as measured by a small tissue-equivalent ionization chamber was found to be 2.2 times the dose at the beam entrance. Measurements of quality factor were 2.7 at the Bragg peak and 3.4 in the middle of the downward slope of the Bragg curve. Their experimental Bragg curve was in good agreement with the calculated curve if the local energy deposition was assumed to be 20 MeV per nuclear star. Further measurements have been made recently by using an LET chamber to measure the contribution of dose due to stars formed by negative-pion capture.[14] Their results at the Bragg-peak position of negative pions indicate that a substantial part of the dose is delivered at LET values appropriate to α particles with energies between 5 and 15 MeV, the peak value of the spectrum being at an LET value appropriate to an α particle of energy[14] 6 MeV. It is quite probable, however, that saturation of their system at high LET prohibited the higher LET portion of the distribution to be accurately measured. A comparison of their spectrum with that in Fig. 3 shows a rather sharp drop to zero in the region where the lower energy α particles should be making a significant contribution.

Dosimetric studies of negative pions have also been carried out at Brookhaven National Laboratory with the negative-pion beam produced at the Cosmotron. The beam had a momentum of 156 MeV/c and a range of about 15 cm in water. The electron and muon contamination of this beam is much higher than the contamination of the CERN and Berkeley beams because very high-energy protons ($\approx$ 2 BeV) from the Cosmotron were used to produce the pion beam, and because the distance between the target and the experimental area was large. Because of the considerable beam contamination, a telescope consisting of particle counters was used for discriminating against the background electronically.[15] A Cerenkov counter was also used for eliminating the dose contribution from the beam contamination, and NaI (Tl) or CsI (Tl) crystals were used as an ionization detector. The ionization spectra were measured as a function of absorber depth. The ionization curve was computed from the pulse-height spectra produced in NaI (Tl) or CsI (Tl) crystals. The data are not yet completely analyzed.

The group from England headed by Peter Fowler has made some calculations of negative-pion dose distributions and the oxygen-enhancement ratio.[5, 10] In addition, they made measurements at the CERN facility of negative-pion capture in oxygen, using wet emulsions as described previously.[10] They do not have a negative-pion beam facility at present for this investigation; however, they are now planning to use Nimrod.

The intensity of the negative pion beam at the 184-inch synchrocyclotron at Berkeley is 5 rads/hr for a beam size of $\approx$ 7 cm by 7 cm. The beam has a contamination of 25% electrons and 10% muons. This beam intensity is two

orders of magnitude lower than that needed for therapeutic application; nevertheless, dosimetric experiments can be done quite well, and with care, limited biological experiments can also. The physical and biological experiments have been done since 1963. A detailed account of the biological experiments will be covered in a separate paper. Most of the physical measurements have already been published,[6-9] and a detailed summary of the results to date will now be given here.

Integral Range Curve

As it passes through the medium, the pion beam is attenuated because of elastic and inelastic interactions with nuclei in the medium. Hence the number of pions passing through an absorber decreases as the thickness of the absorber is increased. This particle loss is important, since the dose at the Bragg-peak position depends on the intensity of the particles there. A plot of the number of particles that reach a given absorber thickness as a function of thickness is called an integral range curve or a number-distance curve. The integral-range measuring apparatus used consists of two plastic scintillators connected in double coincidence to monitor the beam intensity. A third plastic scintillator measures the beam intensity after the particles pass through the variable absorber. The intensity of the transmitted beam through the absorber is given by a triple coincidence between all three scintillators. The integral range curve is the plot of the ratio of the triple coincidences over the double coincidences (incident beam intensity) as a function of the absorber thickness. Such a plot for a pion beam of energy 100 MeV (or momentum 195 MeV/c) with its muon and electron contamination taken in Lucite is shown in Fig. 7. The attenuation of the pion beam before the pions stop is represented by the curve between zero absorber and the point A shown in the figure. Forty percent of the particles from the beam are lost before they reach the pion-stopping region (AB in the figure); the muon and electron contamination is represented from point B onwards. The energy spread and the average energy of the pion beam can be calculated from the integral range curve by taking the energies corresponding to the ranges at points A and B (94.5 and 108 MeV, respectively) from range-energy tables of pions in Lucite. Because of the mass difference between pions, muons, and electrons, for a contaminated pion beam of the same momentum, the muons will have a range 30% greater than pions and the electrons will have a much higher range than muons. Hence, knowing the ranges of pions and muons, we can estimate the contamination of muons and electrons in the pion beam.

Time-of-Flight Measurements

The time-of-flight measurements reveal more vivid information on contamination. In a contaminated pion beam of a given momentum, muons and electrons will travel faster than pions. In these experiments, one measures the time taken by each particle in the beam to travel an extended path (23 feet). A plastic scintillation counter is placed at each end of the flight path. The geometry of this experiment is therefore different from that of the other experiments. The velocity spectrum of the particles, as expressed by the time delay between the two scintillation counters, is fed first to a time-to-pulse-height converter and then to a pulse-height analyzer. Figure 8 shows four Polaroid pictures of the PHA display for a negative-pion beam after it passes through 2-1/8, 6-1/8, 8-5/8, and 13-1/8 inches of Lucite absorber. For absorber thicknesses of 2-1/8 and 6-1/8 inches, the beam is clearly differentiated into three distinct peaks representing the pions, muons, and electrons. Summation of a single peak gives the total number of particles represented by that peak. This procedure was repeated at several different depths in Lucite. The percentage of electrons in the 180 MeV/c beam increases linearly from 23% at the entrance to 40% at the Bragg-peak position in Lucite.

Semiconductor Detector Measurements

Semiconductor detectors are also used for investigating pion beams because of their many advantageous properties, which include their linear response with the deposited energy. A lithium-drifted silicon detector of thickness 0.61 g/cm^2 was employed to analyze both the positive- and negative-pion beams[6] with their contaminants when the particle passed through different depths of Lucite. The experimental details are discussed in an earlier paper.[6]

Figure 9 shows the results obtained with a 95-MeV π^+ beam (189 MeV/c whose muon and electron contamination is very small) after it passed through various thicknesses of Lucite. A number of features of this data are interesting. The resolution is in reasonable agreement with the Landau effect. The peaks are shifted to higher energies by 7-1/2 inches of Lucite, i.e., roughly 1 in. less than the range of pions, a small peak at 1.15 MeV occurs in addition to the 1.98-MeV π^+ peak (Fig. 9b). This small peak is due to μ^+ particles formed by the decay of π^+ mesons. When the beam is degraded by 8-1/2 inches of Lucite, which corresponds to the Bragg-peak position (Fig. 9c), the muon and pion peaks are shifted to higher energies. At 9-1/2 inches of Lucite plus 3/8 inches of copper (copper is used to substitute for a thicker sheet of Lucite because of the lack of space), which is beyond the range of pions and muons, only the positron peak at 0.92 MeV shows (Fig. 9d).

Unlike the π^+ beam, the π^- beam is contaminated with approximately 25% electrons and 10% muons. Figure 10 shows the results obtained with a 95-MeV π^- beam (189 MeV/c) with its muon and electron contamination passing through various thicknesses of Lucite. Two peaks at 0.87 and 1.05 MeV can clearly be seen in Fig. 10(a), and they are due to electrons and pions, respectively. The muon contamination, being relatively small, is hidden in the broad distribution of electrons and pions. Notice that as the absorber thickness increases, the relative height of the pion peak decreases in comparison with the electron peak. This result is due partly to the large loss of pions due to nuclear collisions, and partly to electron build-up due to shower formation. The results of the time-of-flight measurements also confirm this behavior. As the thickness of Lucite increases, the peak due to electrons remains at the position corresponding to about 0.87 MeV, but the peak due to pions shifts to higher energies. This is because the electrons of initial momentum 189 MeV/c are still in the minimum ionizing region, but the pion energy losses increase considerably as the thickness of the Lucite absorber increases. Beyond the range of pions (i.e., for thickness greater than 8-5/8 in. of Lucite), the pion peak is absent and the electron peak persists (Fig. 10d).

The experimental values of the most probable energy losses of pions (both positive and negative) agreed well with the values predicted by theory.

The energy distribution of the negative-pion stars in silicon was also measured. Using ionization chambers, we obtained the Bragg peak at 8-5/8 in. of Lucite. Most of the pions stop in this region and create stars. Hence, a lithium-drifted silicon detector placed at this position will stop many negative pions, and stars will be formed in silicon. Most of the star's energy will be absorbed in the detector itself. In order for the detector to "see" the energy distribution of the pion stars alone, the energy deposited by the pions, muons, and electrons while passing through the detector has to be eliminated. This elimination is done with another semiconductor detector in anticoincidence with the analyzing detector. The results of such measurements are shown in Fig. 11. It can be seen from the figure that the number of stars is constantly decreasing with increasing energy, and this star energy extends beyond 60 MeV. The computed average energy of the star stopped in detector (0.61 g/cm^2) is 21 MeV.

Depth-dose Distribution of Pion Beams

Our early measurements were made by using two 7-in. diameter ionization chambers filled with a mixture of 96% argon and 4% carbon dioxide, at a pressure of 3 psi over atmospheric pressure. The depth-dose distribution of pion beams was measured by using one chamber as monitor, followed by different thicknesses of Lucite absorber, and then using the second chamber as a detector. Measurements were made for beams of both positive and negative pions. The Bragg peak due to the negative-pion beam should be enhanced due to the pion stars when compared with that from a positive-pion beam of the same energy. However, the Bragg ratio for both positive and negative pion beams was found[7] to be 2:1. This is partly due to the differences in the contamination for positive- and negative-pion beams. Also, because the positive-pion beam decayed into muons and positrons near the Bragg-peak position, the ionization chamber, being larger than the beam, will "see" more ionization from these long-range products than from the short-range star products from the negative-pion beam.

In addition to the depth-dose distribution of pion beams, it is important to measure also the ionization density at the points of interest. Lithium-drifted silicon detectors are also being used for such measurements by operating them as pulse-radiation dosimeters.[8]

The charge liberated in the lithium-drifted silicon detector is directly proportional to the energy deposited in it. A charge-sensitive preamplifier yields a voltage pulse proportional to the energy deposited in the detector. At room temperature, the leakage current of the lithium-drifted silicon detector is $\approx 2\ \mu A$, depending on the thickness of the detector, and this current is comparable to the current generated in the detector due to pions passing through it. (The total pion intensity seen by the detector is 10^4/sec). The detector leakage current has been blocked by ac amplification used in the system, as shown in the block diagram in Fig. 12. Simple capacitive coupling is not adequate because of cancellation of the positive signal by the negative overshoot. This cancellation necessitates a polarity-clipping circuit to eliminate the overshoot contribution to the subsequent integration. The integration consists of a standard operational amplifier with feedback capacitor. It is electronically reset by a diode pump that furnishes an accurate amount of charge to the capacitor. To measure the dose due to pulses corresponding to the energy deposition in the detector greater than a particular value or over a particular range of energies, we used a single-channel pulse-height analyzer (or discriminator), gated linear amplifier, and a delayed amplifier. Such threshold measurements yield information on the distribution of ionization density at the measured position.

This system was used to measure the depth-dose distribution of a 190 MeV/c pion beam in water. The most probable energy losses in the 3-mm detector used in this investigation are 1 MeV by the electrons and 1.2 MeV by the pions, and the energy lost by the muons is intermediate between these values. At the end of the range the negative pions stop and produce stars, thereby depositing in the detector energies at times exceeding 60 MeV. Hence the systems should be linear at least from 0.6 MeV to 60 MeV. When checked out with a calibrated pulser, the system was found to be linear within 5% over the energy region from 0.6 to 60 MeV.

Two plastic scintillators connected in coincidence were used to monitor the fluctuating pion beam. The lithium-drifted silicon detector was housed in a small waterproof Lucite-box and could be moved remotely in a water phantom. The integrated charge from the lithium-drifted silicon detector was measured during the time the monitor scintillator system accumulated a fixed number of counts. This procedure was repeated for each position of the detector in the

water phantom. For comparison, measurements were also made for a positive-pion beam, with the results shown in Fig. 13. As can be seen from the figure, the negative-pion beam gave rise to a much higher dose than that of the positive-pion beam near the end of the range.

The depth-dose distribution of a negative-pion beam in water as measured with a silicon detector agreed reasonably well with the calculated dose in water shown in Fig. 4. The similarity between the two results indicates that the nuclear interactions occurring when pions are captured in silicon do not produce significantly different particle types and spectra from those occurring in water. Thus, silicon detectors appear to be useful dosimeters for these investigations, although the dose measured is not strictly the tissue dose.[12]

The integrated output of the lithium-drifted silicon detector was measured as a function of the discriminator setting (energy threshold) for positions designated 1, 2, 3, and 4 in Fig. 13. For comparison, the integrated output of the detector at zero threshold setting of the discriminator at the above-mentioned positions was normalized to unity. The resulting curves are shown in Fig. 14.

The two curves for the negative-pion beam at positions 1 and 2 corresponding to the peak and halfway down the falling portion of the depth-dose distribution curve are similar, thereby suggesting that the ionization density distributions at and beyond the peak of the negative-pion depth-dose curve may be similar. On the other hand, the curve corresponding to the position 3 halfway up the rising slope of the depth-dose curve falls below curves 1 and 2 with increasing threshold setting, thereby suggesting that the contribution from high ionization densities at that point is considerably less than at the other two points. As expected, the fractional dose for threshold settings greater than 10 MeV at position 4 of the positive-pion peak falls to zero quickly, as there are no stars contributing to the dose here. For the detector thickness used (3 mm), pulses greater than about 9 MeV cannot be due to the passage of pions through the detector. For negative pions, pulses greater than 9 MeV are definitely due to star formation and, as can be seen from Fig. 14, the stars contribute about 60% of the dose at the Bragg peak position.

It will be better to use thin detectors for measuring the depth-dose distribution because of the narrow width of the region where negative pions produce stars ($\approx$ 4 cm of water). Improvements in the linearity of the system are being made so as to permit use of thinner detectors. The depth-dose curve for a pure pion beam can be obtained by using a threshold Cerenkov counter in anticoincidence with the semiconductor detector so that the particles with velocities greater than pions (i.e., muons and electrons) will not be counted. Work in this direction is also in progress.

The electron contamination in the pion beam can be reduced considerably by using electrostatic separators; however, the existing muon contamination is relatively difficult to eliminate because its mass is nearly that of pion. Muons will deliver some radiation dose beyond the region of interest. The best way to minimize the muon contamination of the pion beams is to keep the experimental area a close to the target as possible. This will decrease the flight path of the pions, and hence fewer pions will decay into muons.

The results of the physical measurements and calculations indicate that the negative-pion beams may find a good place in radiation therapy. As mentioned before, the intensity of the presently available pion beams is two orders of magnitude lower than that needed for therapeutic application. Construction of machines that produce the necessary intensities is being planned, and one such machine is being considered for Los Alamos Scientific Laboratory with a special biomedical facility.

References

1. J. H. Lawrence, P. C. Abersold, and E. O. Lawrence, Comparative Effects of X-rays and Neutrons on Normal and Tumor Tissue, Proc. Natl. Acad. Sci. U.S. 22:543 (1936).
2. J. F. Fowler, Neutrons in Radiotherapy: Slow Neutrons, Fast Neutrons and Other Heavy Particles, Biological Effects of Neutron and Proton Irradiation, Vol. II, IAEA, page 185 (1964).
3. M. R. Raju, Heavy Particle Studies Using Silicon Detectors, USAEC Report, UCRL-16354, Lawrence Radiation Laboratory, August 1965; also in Proceedings of the Workshop Conference on Space Radiation Biology, Berkeley, California, Sept. 1965 (to be published in Rad. Res.).
4. The Omnitron — A Multipurpose Accelerator, USAEC Report, UCRL-16828, Lawrence Radiation Laboratory, July 1966.
5. P. H. Fowler and D. H. Perkins, The Possibility of Therapeutic Applications of Beams of Negative π-Mesons, Nature 189: 524 (1961).
6. M. R. Raju, H. Aceto, and C. Richman, Pion Studies with Silicon Detectors, Nucl. Instr. Methods 37: 152 (1965).
7. C. Richman, H. Aceto, M. R. Raju, and B. Schwartz, The Radiotherapeutic Possibilities of Negative Pions, Am. J. Roentogenol. Radium Therapy Nucl. Med. XCV1: 777 (1966).
8. M. R. Raju, E. J. Lampo, S. B. Curtis, J. M. Sperinde, and C. Richman, Lithium-Drifted Silicon Detector Used as a Pulse Dosimeter, USAEC Report, UCRL-16924, Lawrence Radiation Laboratory, Sept. 1966; also presented at the 13th Nuclear Science Symposium on Instrumentation in Space and Laboratory, Boston, Massachusetts, Oct. 19-21, 1966 (proceedings to be published by IEEE).
9. Henry Aceto, A Feasibility Study of the Therapeutic Possibilities of π-Mesons, USAEC Report, UCRL-11482, Lawrence Radiation Laboratory, June 1964.
10. P. H. Fowler, π Mesons Versus Cancer, Proc. Phys. Soc. (London) 85: 1051 (1965).
11. P. Ammiraju and L. M. Lederman, Diffusion Chamber Study of Very Slow Mesons. IV. Absorption of Pions in Light Nuclei, Nuovo Cimento 4: 283 (1956).
12. S. B. Curtis, M. R. Raju, and C. Richman, to be published.
13. J. Baarli, Radiological Physics of Mesons, to be published in the Proceedings of the Work Shop Conference on Space Radiation Biology, Berkeley, California, Sept. 1965 (to be issued as a Special Supplement to Rad. Res.).
14. T. R. Overton, Experience with a Linear Energy Transfer (LET) Chamber at CERN, CERN Report CERN 66-33, October 1966.
15. G. M. Tisljar-Lentulis, Method for Measurement of Ionization Curves by Means of Scintillation Counters, Rev. Sci. Instr. 37: 291 (1966).

Figure Legends

Fig. 1. Examples of π^+ decay as observed in nuclear emulsions. From C. F. Powell, P. H. Fowler, and D. H. Perkins, The Study of Elementary Particles by the Photographic Method, p. 669, Pergamon Press, N. Y., 1959.

Fig. 2. Disintegration of light elements carbon, nitrogen, or oxygen by nuclear capture of π^- mesons as observed in nuclear emulsions. The pion tracks are labelled π^-; the stars produced following their capture have various numbers of prongs. From C. F. Powell, P. H. Fowler, and D. H. Perkins, The Study of Elementary Particles by the Photographic Method, p. 669, Pergamon Press, N. Y., 1959.

Fig. 3. Calculated energy-loss distribution at a point in the stopping negative-pion region in 25.5 cm of water. P = 190±5 MeV/c.

Fig. 4. Calculated central-axis depth-dose distribution of negative-pion beam with its contaminants in water. P = 190±5 MeV/c. Incident beam is 65% pions, 25% electrons, and 10% muons.

Fig. 5. Calculated central-axis depth-dose distribution in water of pure negative-pion beams. P = 190±5 MeV/c.

Fig. 6. Experimental setup for producing a negative-pion beam. For producing a positive-pion beam, all the magnetic fields and the direction of the proton beam are also reversed.

Fig. 7. Integral range curve of a negative 100-MeV pion beam.

Fig. 8. Time-of-flight pictures of pion beam with its contaminants after passing through 2-1/8, 6-1/8, 8-5/8, and 13-1/8 inches of Lucite.

Fig. 9. Pulse-height spectra from lithium-drifted silicon detector for a 95-MeV π^+ beam after passing through various thicknesses of Lucite. (a) Direct beam; (b) beam degraded by 7.5 inches of Lucite; (c) beam degraded by 8.5 inches of Lucite; (d) beam degraded by 9.5 inches of Lucite and 3/8 inch of copper.

Fig. 10. Pulse-height spectra from a lithium-drifted silicon detector for a 95-MeV π^- beam with its contaminants after passing through various thicknesses of Lucite. (a) Direct beam; (b) beam degraded by 3 inches of Lucite; (c) beam degraded by 5 inches of Lucite; (d) beam degraded by 10 inches of Lucite.

Fig. 11. Energy distribution of the negative-pion endings in silicon; this is very nearly the energy distribution of the pion stars. The curve without the anticoincidence detector includes the pulses of particles passing through but not stopping in the analyzer detector.

Fig. 12. Block diagram of the pulse radiation dosimeter setup.

Fig. 13. Measured central-axis depth-dose distribution of 190-MeV/c π^+ and π^- beam in water.

Fig. 14. Fraction of dose due to particles depositing energies higher than the threshold energy setting, shown as a function of threshold energy.

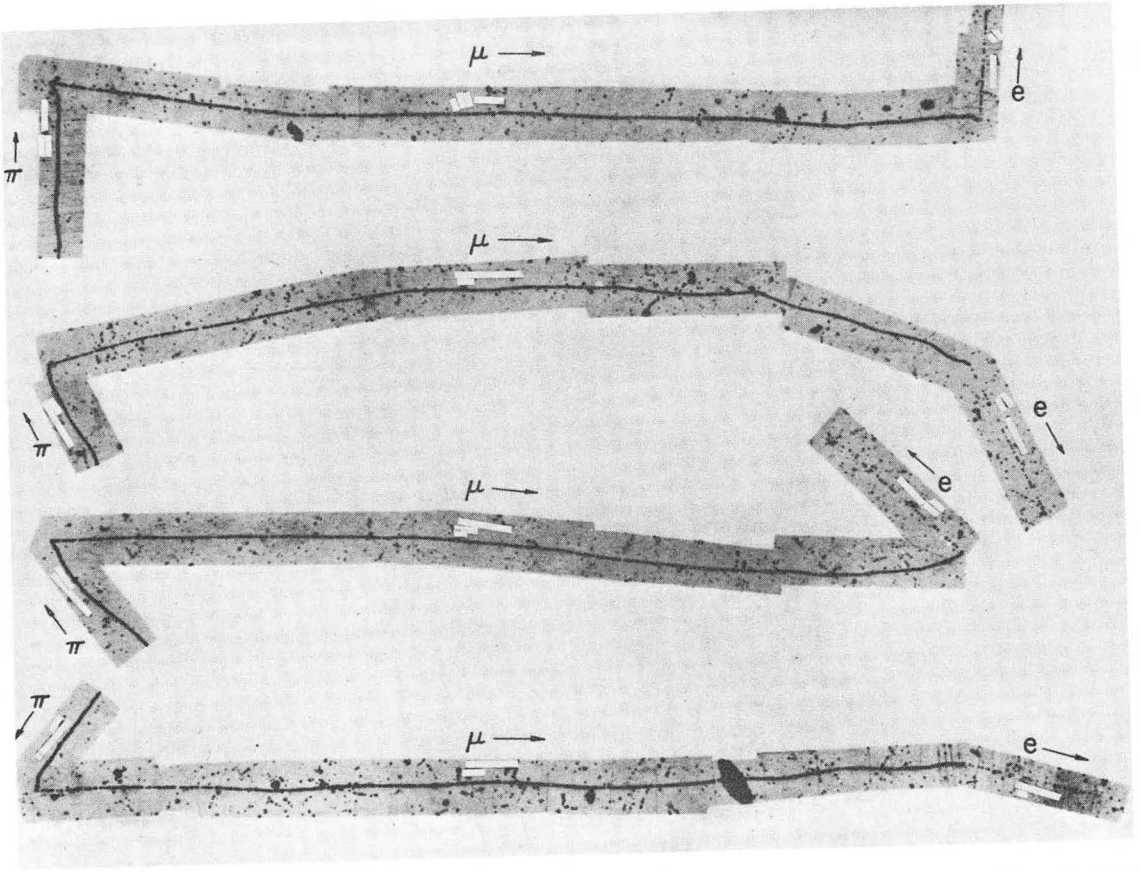

JHL 4962A

Fig. 1

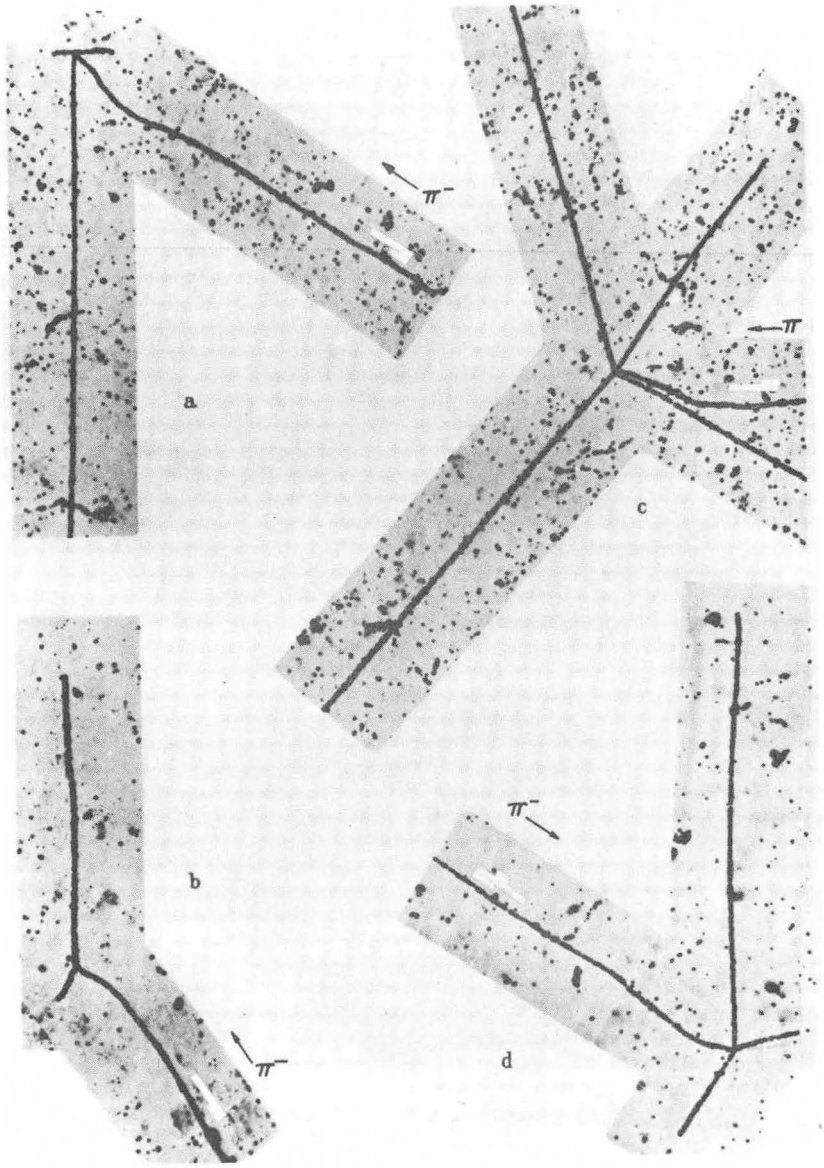

XBB 673-1162A

Fig. 2

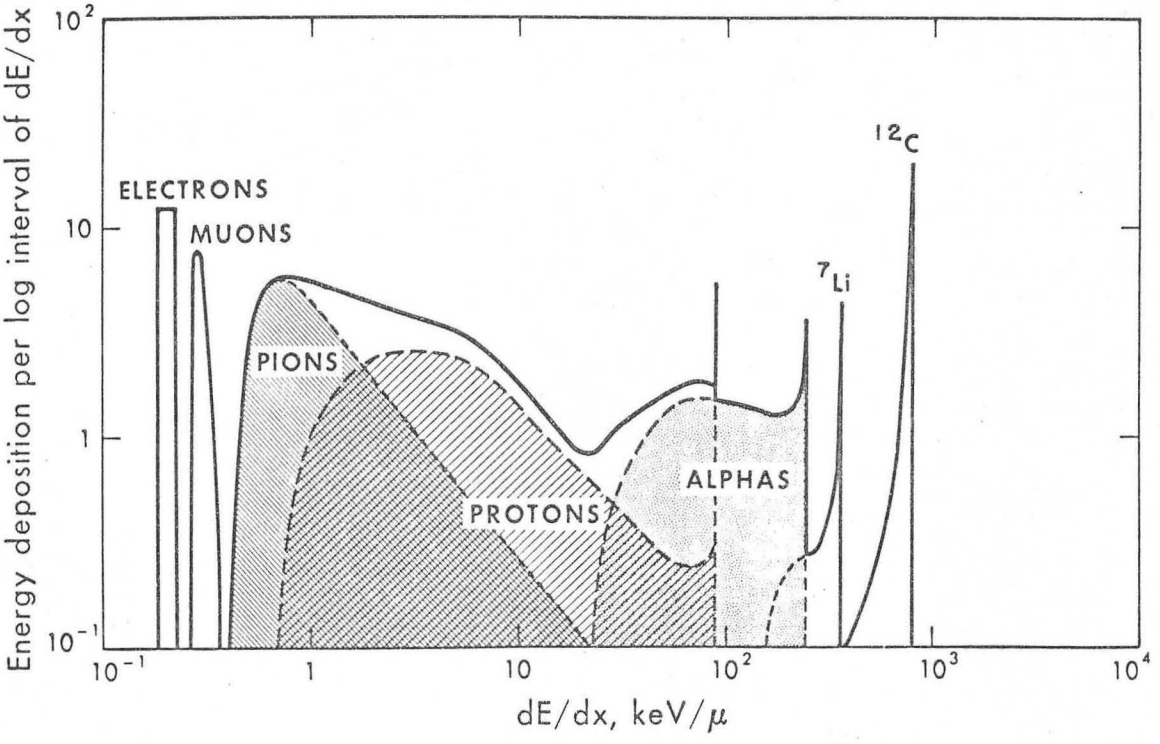

XBL 673-1231A

Fig. 3

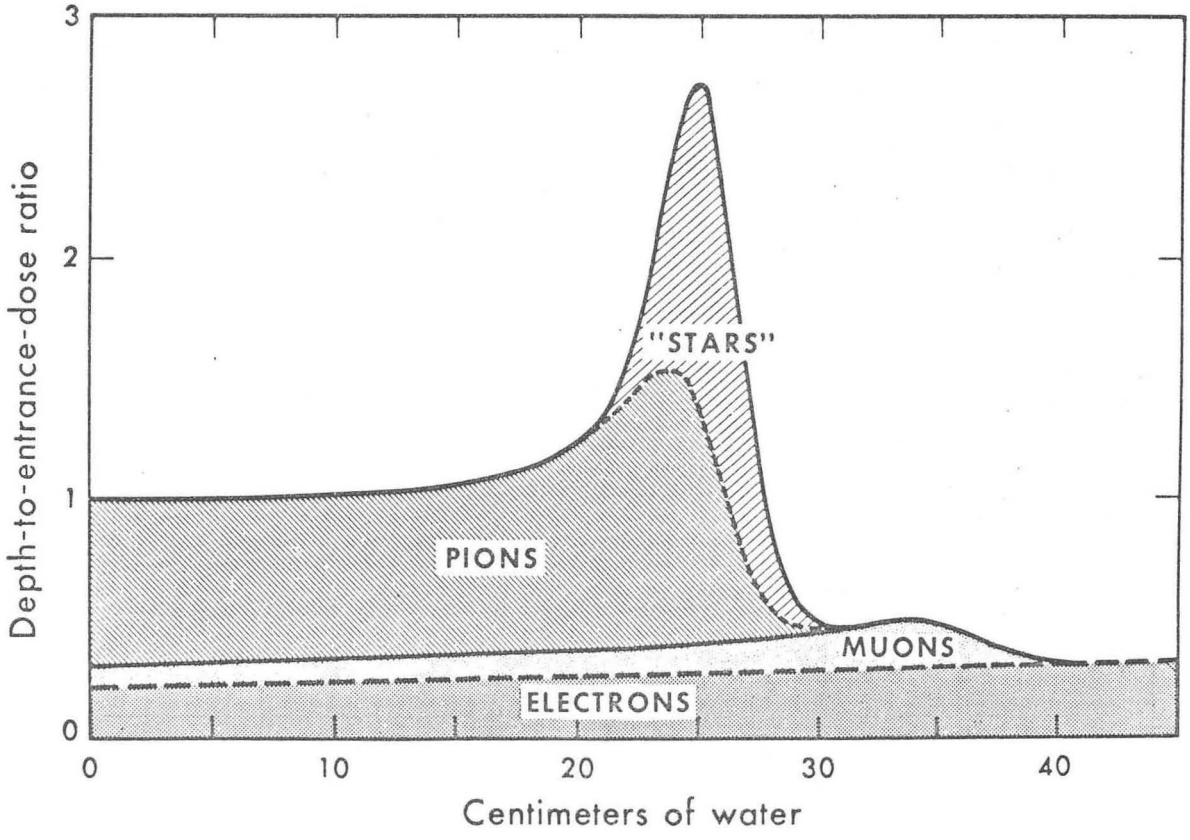

XBL 673-1230A

Fig. 4

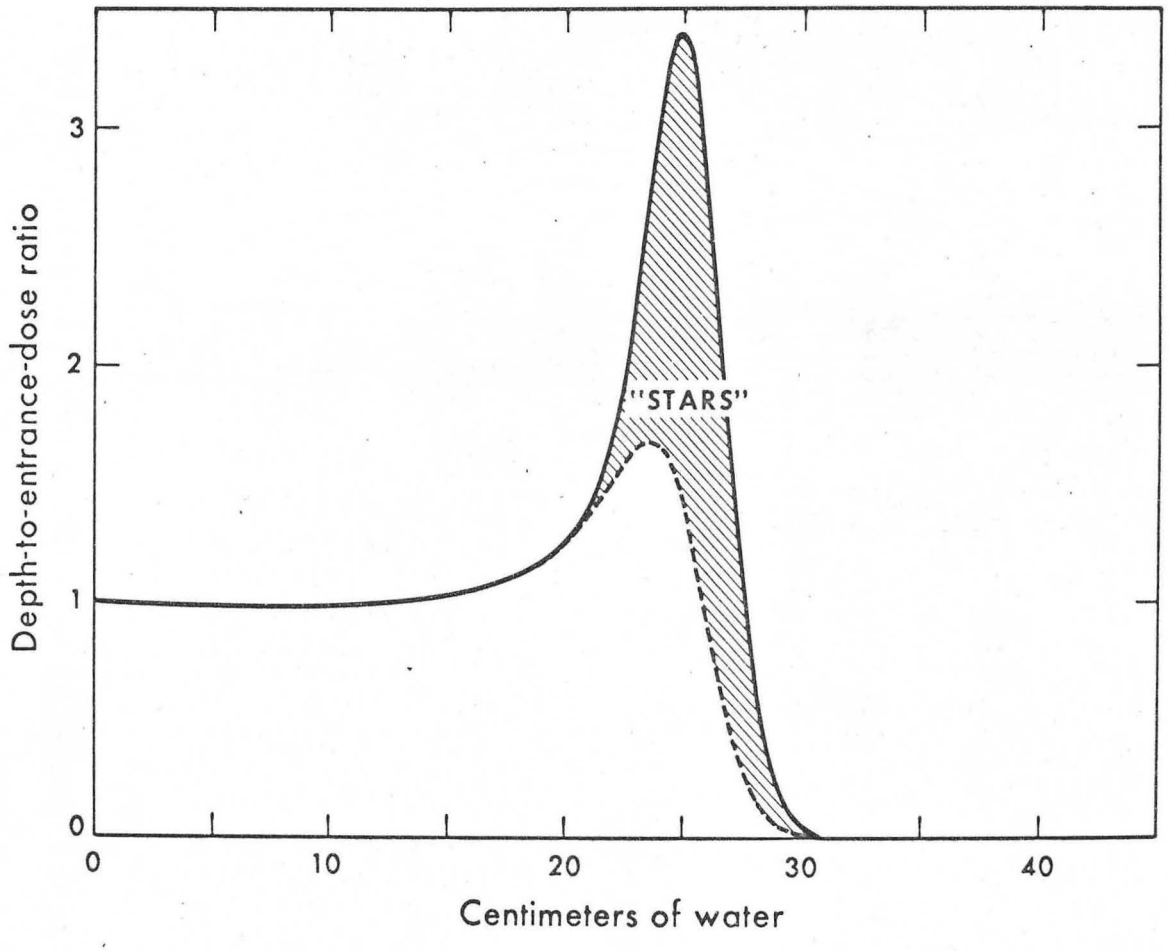

XBL 673-1229A

Fig. 5

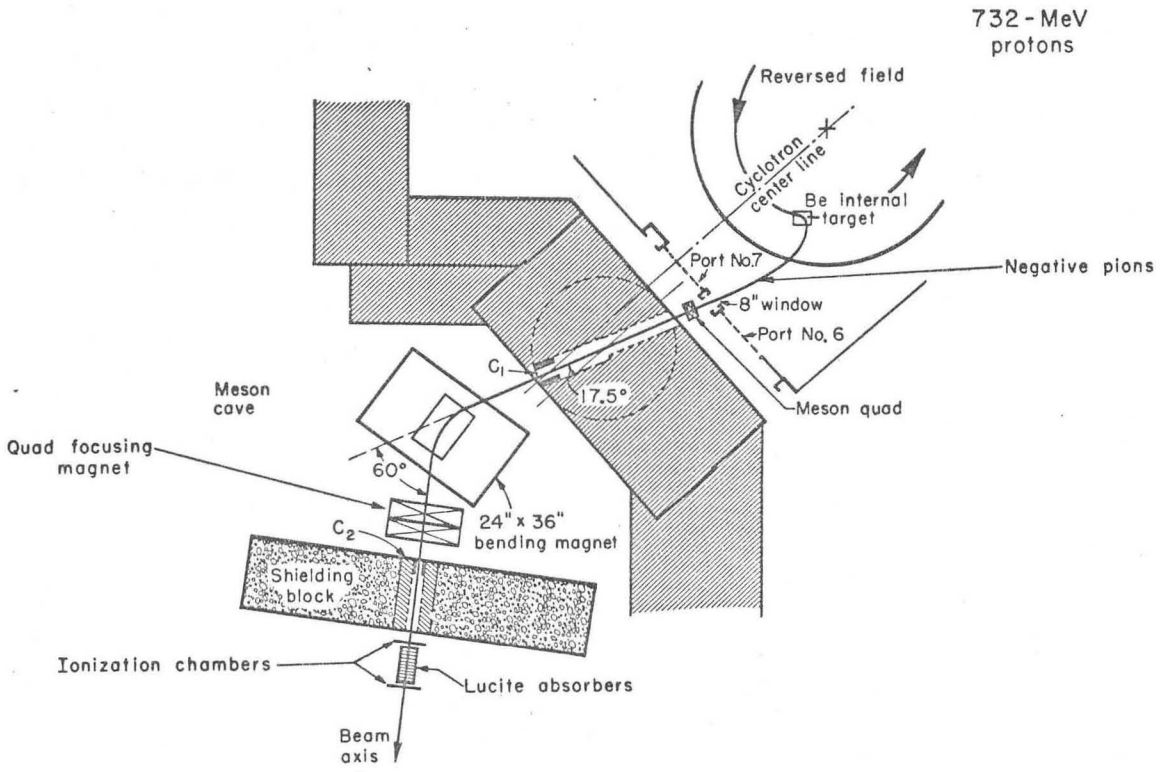
732-MeV
protons
Reversed field
Cyclotron
center line
Be internal
target
Port No.7
Negative pions
8" window
Port No. 6
Meson quad
C_1
17.5°
Meson
cave
Quad focusing
magnet
60°
24" x 36"
bending magnet
C_2
Shielding
block
Ionization chambers
Lucite absorbers
Beam
axis
MUB-966

Fig. 6

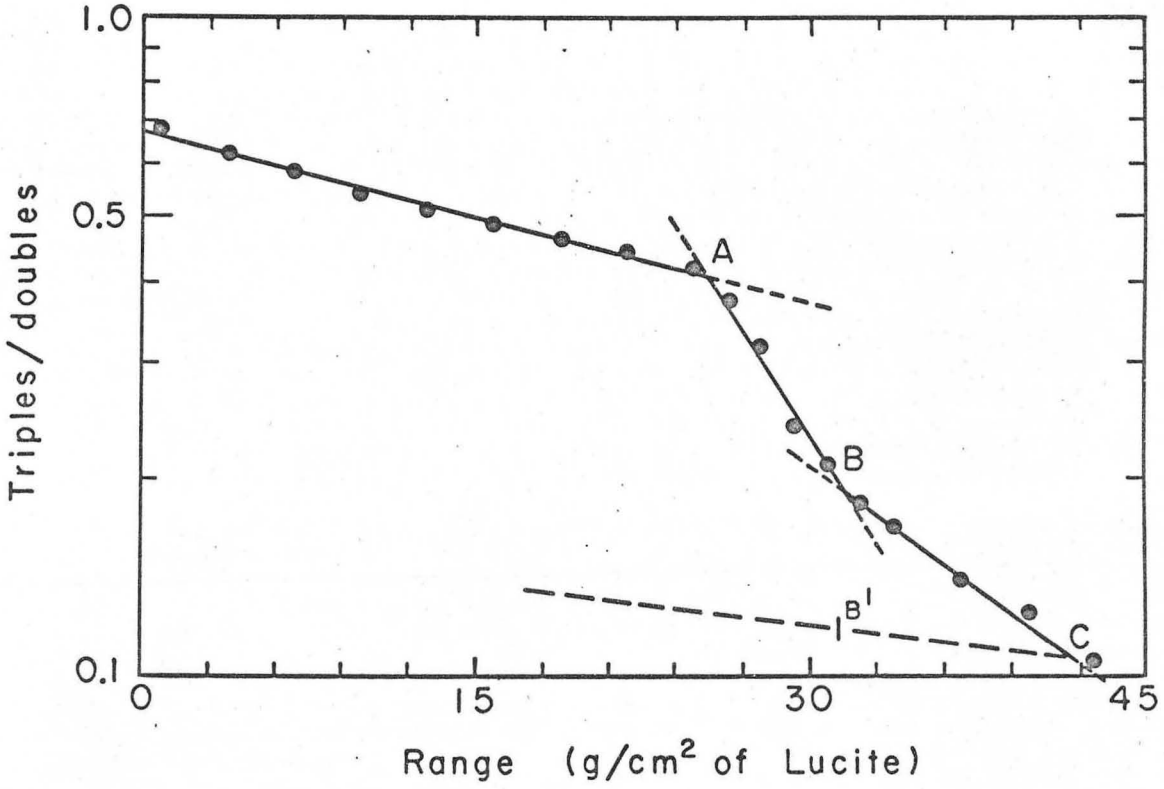
1.0
0.5
0.1
Triples/doubles
0
15
30
45
Range (g/cm² of Lucite)
A
B
B'
C
MU-34178

Fig. 7

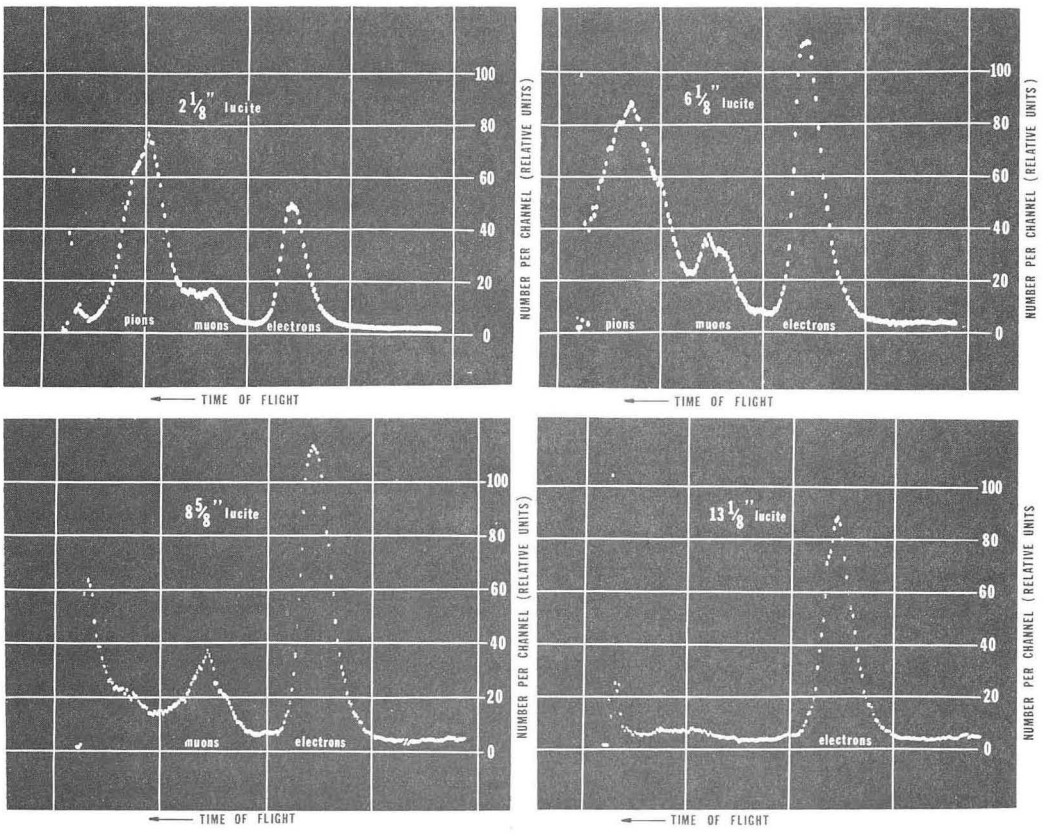
2 1/8" lucite
pions
muons
electrons
6 1/8" lucite
pions
muons
electrons
8 5/8" lucite
muons
electrons
13 1/8" lucite
electrons
NUMBER PER CHANNEL (RELATIVE UNITS)
100
80
60
40
20
0
TIME OF FLIGHT

ZN-5090

Fig. 8

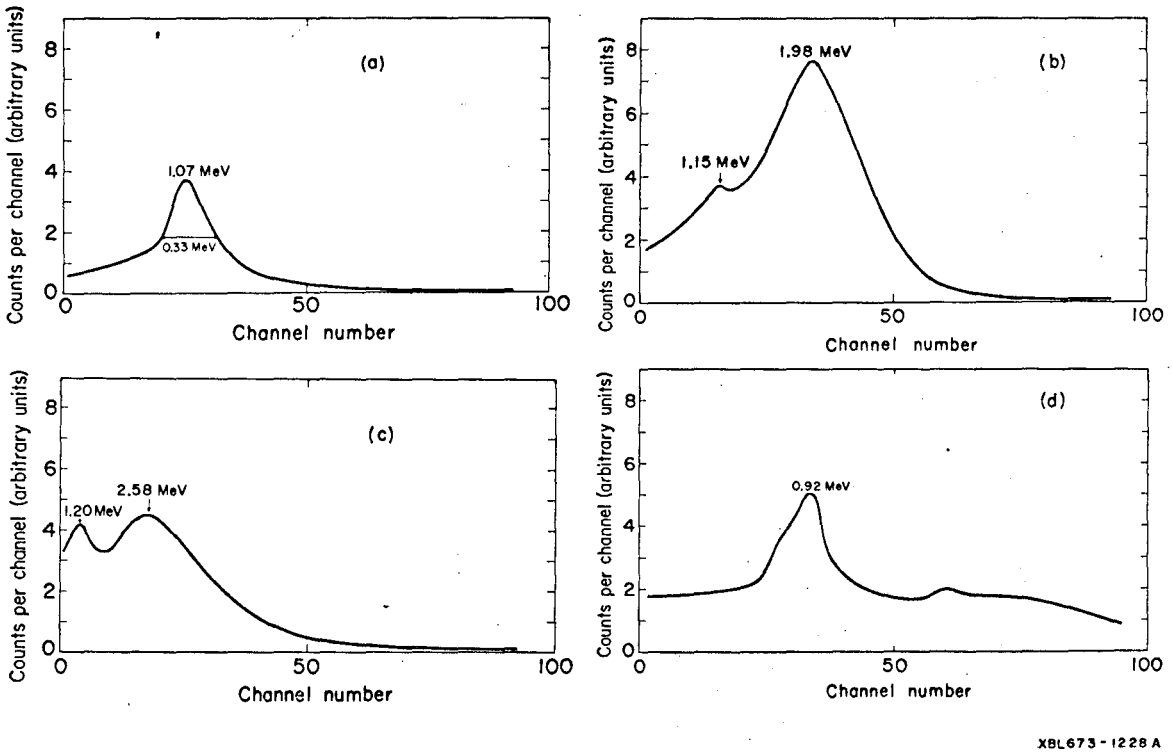
(a)
1.07 MeV
0.33 MeV
(b)
1.98 MeV
1.15 MeV
(c)
2.58 MeV
1.20 MeV
(d)
0.92 MeV
Counts per channel (arbitrary units)
Channel number
0
50
100
2
4
6
8
XBL673-1228A

Fig. 9

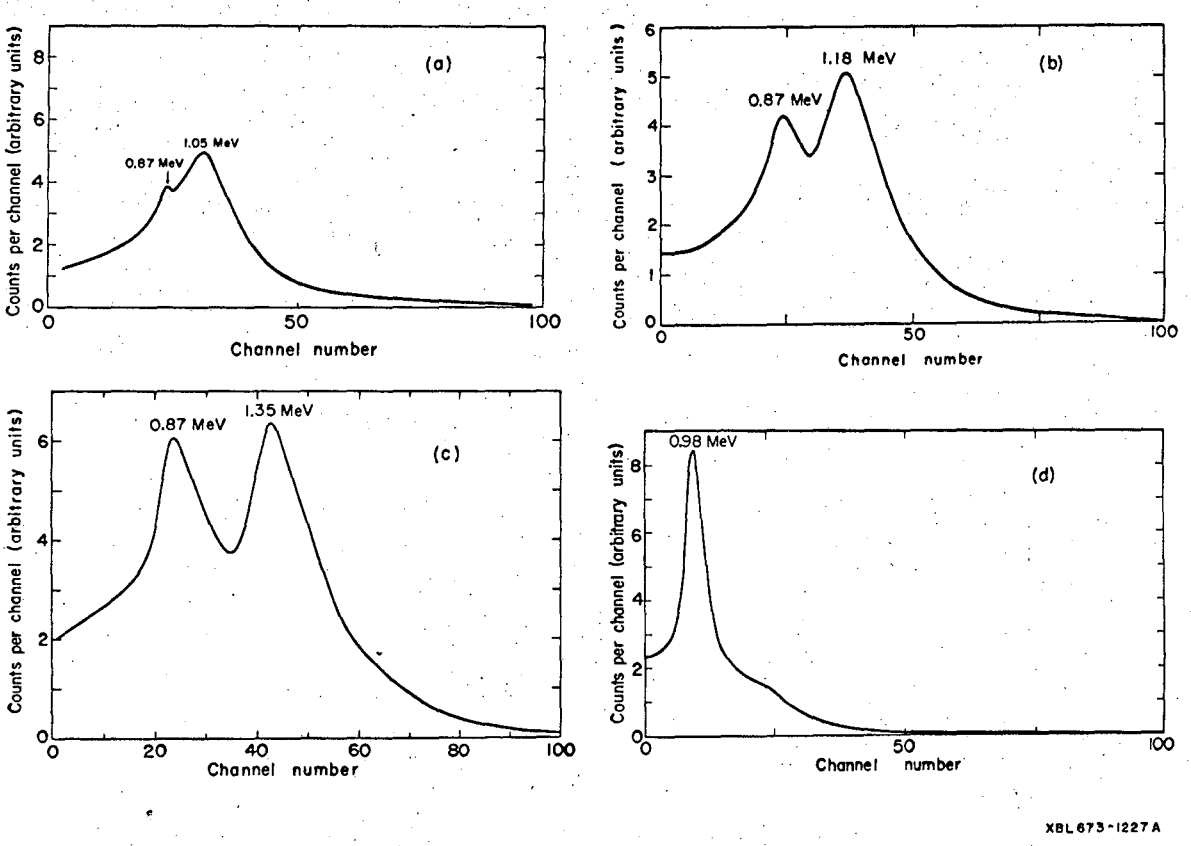
(a)
0.87 MeV
1.05 MeV
Counts per channel (arbitrary units)
Channel number
(b)
0.87 MeV
1.18 MeV
Counts per channel (arbitrary units)
Channel number
(c)
0.87 MeV
1.35 MeV
Counts per channel (arbitrary units)
Channel number
(d)
0.98 MeV
Counts per channel (arbitrary units)
Channel number
XBL673-1227A

Fig. 10

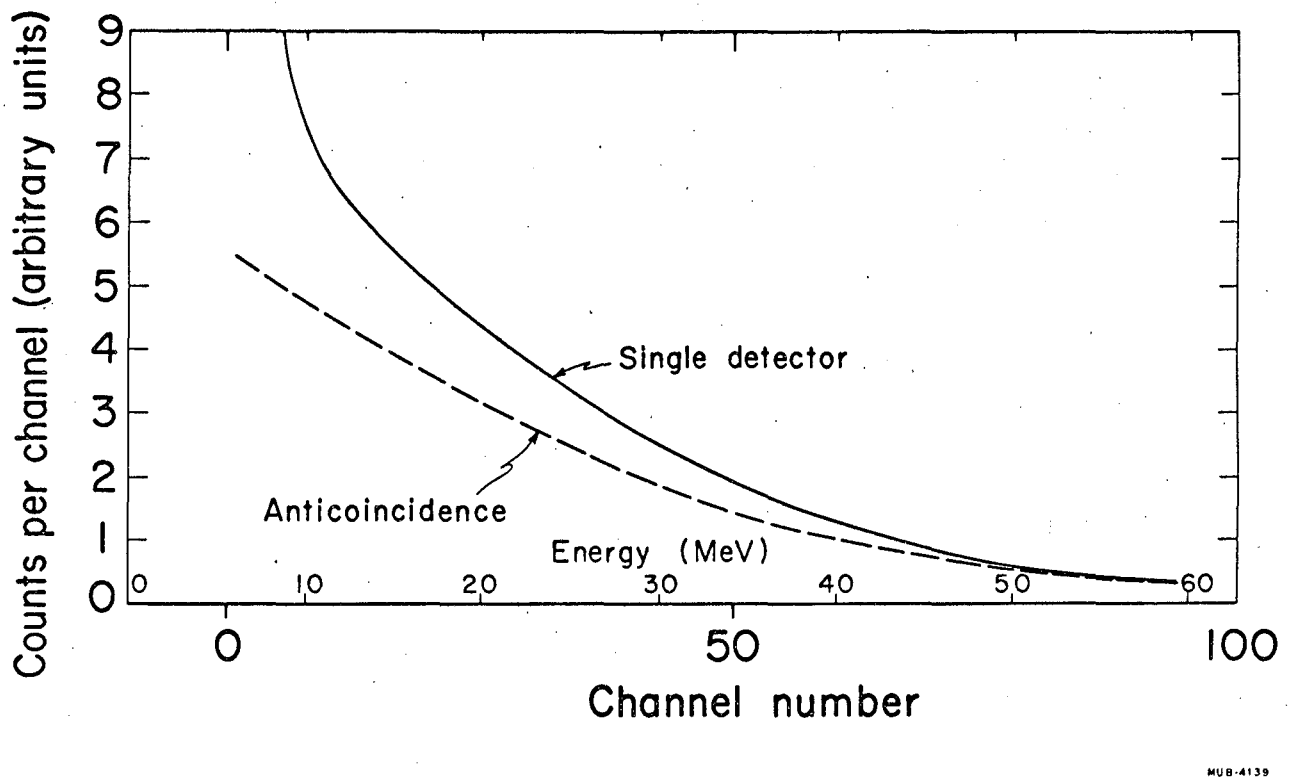
Counts per channel (arbitrary units)
9
8
7
6
5
4
3
2
1
0
Single detector
Anticoincidence
Energy (MeV)
0
10
20
30
40
50
60
0
50
100
Channel number
MUB-4139

Fig. 11

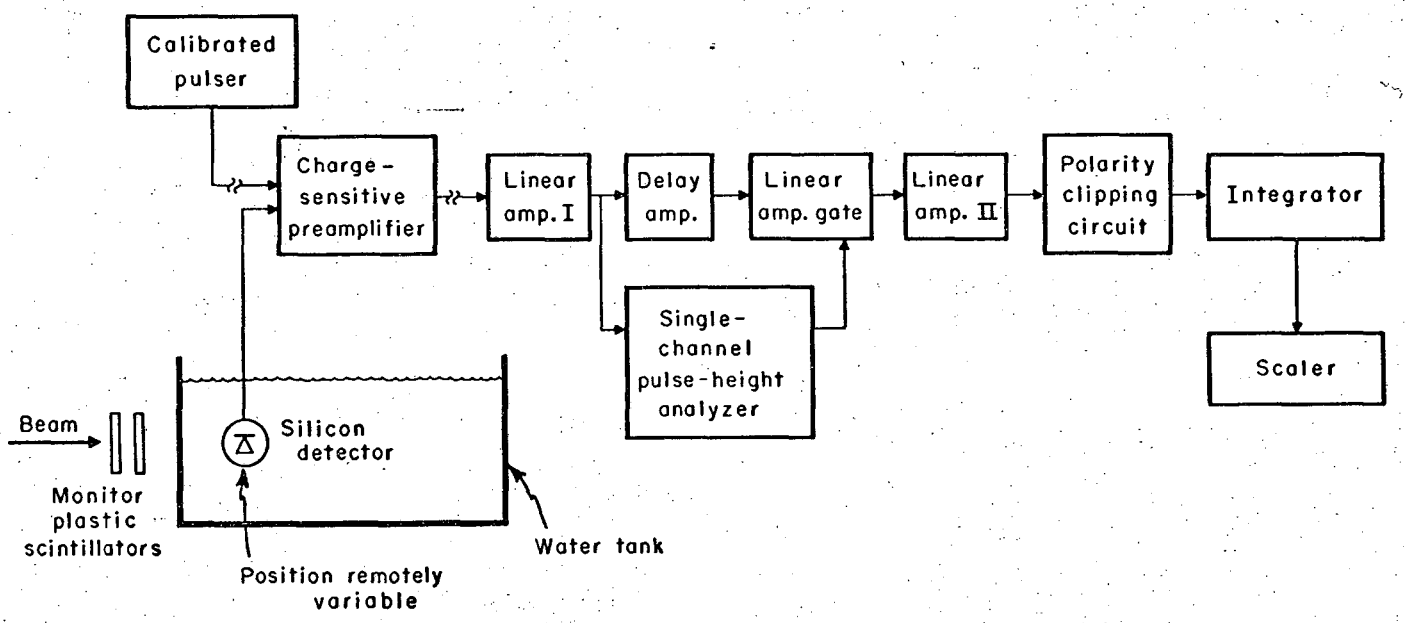

MUB-12915

Fig. 12

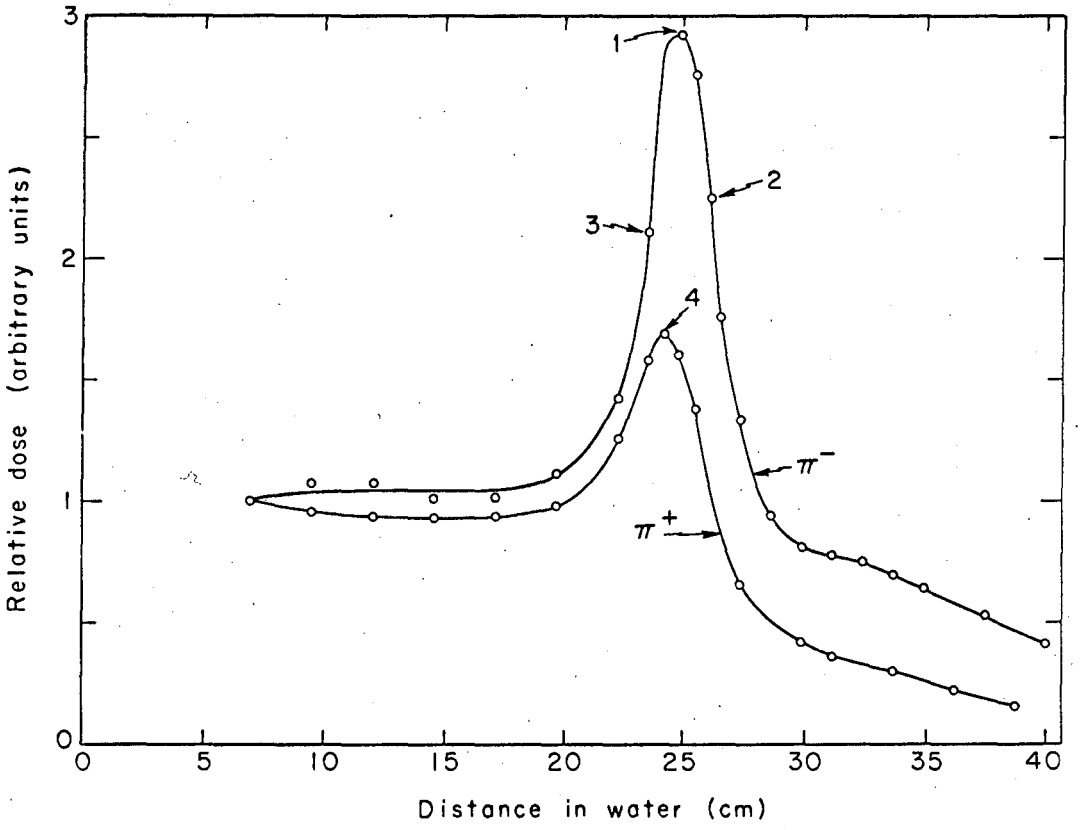
Relative dose (arbitrary units)
Distance in water (cm)
0
1
2
3
0
5
10
15
20
25
30
35
40
1
2
3
4
π⁻
π⁺
MUB-12917

Fig. 13

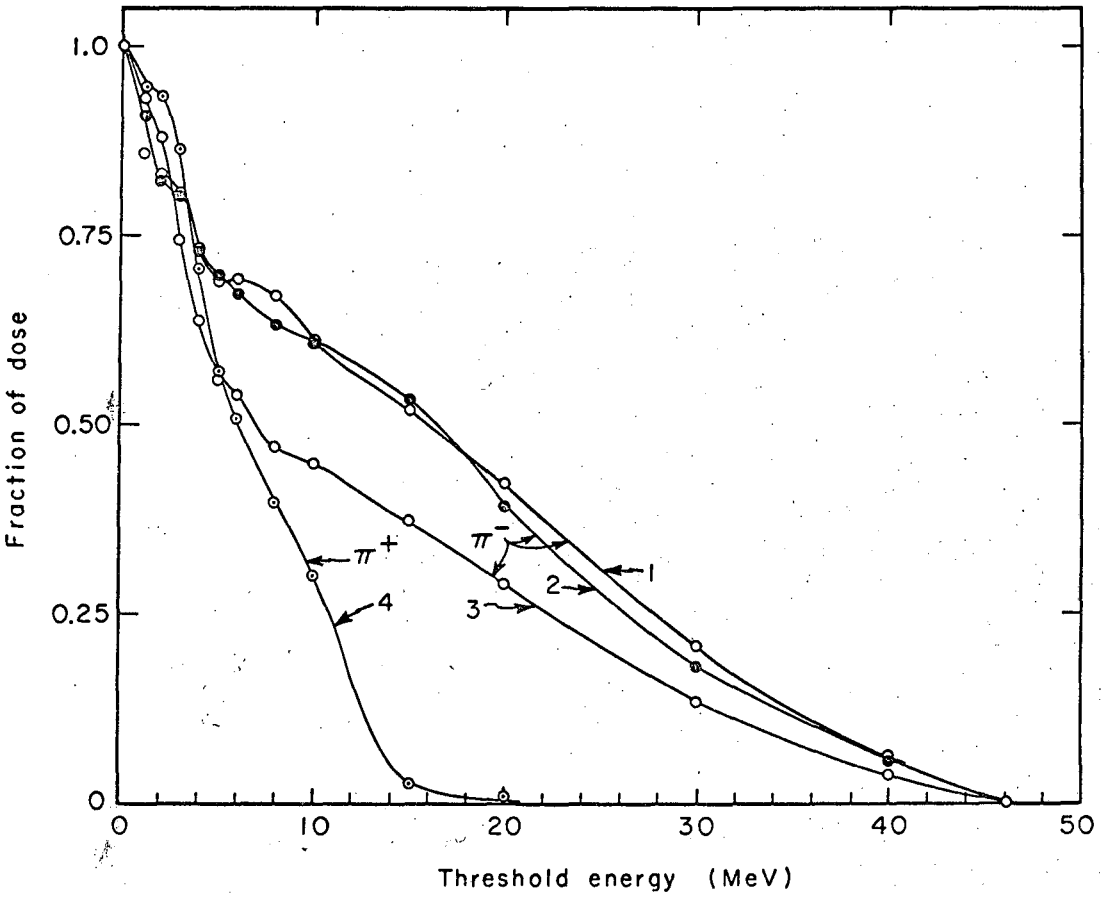
1.0
0.75
0.50
0.25
0
Fraction of dose
0
10
20
30
40
50
Threshold energy (MeV)
π+
π−
1
2
3
4
MUB-12916

Fig. 14